

# Hydrodynamic Simulations of Long-Scale-Length Plasmas for Two-Plasmon–Decay Planar-Target Experiments at the National Ignition Facility

## Introduction

Coronal plasmas of direct-drive–ignition designs with a baseline plastic ablator are characterized by long density scale lengths  $L_n \sim 500$  to  $600 \mu\text{m}$ . Understanding and controlling the impact of laser–plasma interaction (LPI) instabilities in such plasmas are key requirements of inertial confinement fusion (ICF) research. One of the instabilities driven by multiple laser beams that can exceed the instability threshold is two-plasmon decay (TPD).<sup>1–4</sup> In TPD, the overlapping intense laser beams excite large-amplitude electron plasma waves in the region near the quarter-critical density ( $n_{qc}$ ) surface, leading to extra laser absorption and hot-electron production. The extra absorption at  $n_{qc}$  may reduce, however, the laser intensity reaching critical density, thereby decreasing the hydroefficiency. The hot-electron generation from TPD may negatively affect target compression because of the possible preheat of the imploding shell, which must remain on a low adiabat for efficient compression. Other LPI instabilities, such as multibeam stimulated Raman scattering (SRS), can also lead to anomalous laser-energy dissipation before the  $n_{qc}$  surface and/or hot-electron generation.

To support direct-drive ICF experiments at the National Ignition Facility (NIF) in its indirect-drive beam configuration, the polar-direct-drive (PDD) concept was proposed.<sup>5</sup> The impact of laser parametric instabilities on the PDD implosions has been recently tested in experiments on the NIF.<sup>6</sup> To investigate the scaling of TPD-induced hot electrons to the laser intensity and plasma conditions, a series of planar experiments has also been conducted at the Omega Laser Facility.<sup>7</sup> The plasma parameters at the  $n_{qc}$  surface achieved in those experiments (as predicted by simulations using the code *DRACO*<sup>8</sup>) are

summarized in Table 145.II. The coronal plasma parameters in the NIF PDD-ignition design developed at the Laboratory for Laser Energetics<sup>9</sup> are also shown. Table 145.II shows that all parameters in the previous experiments [the overlapped laser intensity ( $I$ ), density scale length ( $L_n$ ), and electron temperature ( $T_e$ ) at the  $n_{qc}$  surface] are still  $\sim 1.5$  to  $2\times$  below that in the ignition design. The empirical TPD threshold parameter  $\eta = I_{14} L_n / (230 T_e)$ , often used to evaluate the effect of TPD,<sup>2,10</sup> is  $\sim 2\times$  less than in the ignition design. Importantly, cross-beam energy transfer (CBET) reduces the laser beam energy, reaching the  $n_{qc}$  surface in current NIF implosion experiments, so that current implosion experiments do not achieve ignition-relevant coronal plasma conditions.

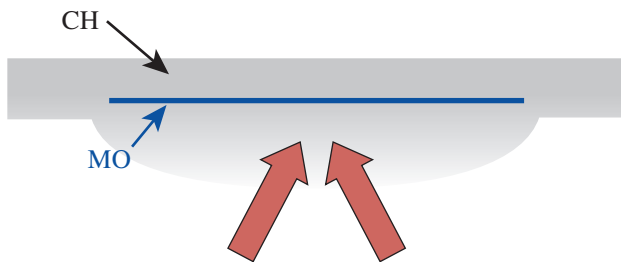
In this article, hydrodynamic simulations using *DRACO* are presented to show that coronal plasma conditions in the ignition PDD design can be approached in planar-target experiments on the NIF (Table 145.II). Since planar targets exhibit a very high absorption efficiency, CBET seeded by backscattered light represents a negligible source of losses in laser energy. It is speculated that because of the characteristics of the NIF beam overlap on the target, the TPD instability will be able to share decay waves most effectively along the polar axis and around the equatorial region of a PDD implosion. Two planar-target simulations that differ by the NIF beam irradiation geometry are presented: (1) irradiation by the NIF inner-cone beams only ( $23.5^\circ$  and  $30^\circ$  incidence angle with respect to target normal) and (2) irradiation by the outer-cone beams ( $44.5^\circ$  and  $50^\circ$ ). The higher-angle cones approximate irradiation conditions near the equator of a PDD implosion, while the lower-angle cones correspond to those near the poles.

Table 145.II: Plasma parameters at the  $n_{qc}$  surface and two-plasmon–decay (TPD) threshold in OMEGA and NIF experiments, ignition NIF PDD design, and planar targets in this article, as predicted by *DRACO* simulations.

Parameters at $n_{qc}$ surface	OMEGA	Current NIF PDD	Ignition NIF PDD	Planar NIF
$I$ ( $\text{W}/\text{cm}^2$ )	$<4 \times 10^{14}$	$<4.5 \times 10^{14}$	$8 \text{ to } 10 \times 10^{14}$	$6 \text{ to } 8 \times 10^{14}$
$L_n$ ( $\mu\text{m}$ )	$<350 \mu\text{m}$	$<350 \mu\text{m}$	$600 \mu\text{m}$	$550 \text{ to } 600 \mu\text{m}$
$T_e$ (keV)	$<2.5 \text{ keV}$	$<3.5 \text{ keV}$	$5 \text{ keV}$	$3.2 \text{ keV}$
$\eta$	$<2.4$	$<2$	$4.7$	$4.5 \text{ to } 5.5$

### Proposed Experimental Configuration

The planar-target design is shown schematically in Fig. 145.17. The target is an  $\sim 5$ -mm-diam,  $\sim 500$ - $\mu\text{m}$ -thick plastic CH disk. A  $30$ - $\mu\text{m}$ -thick,  $\sim 4$ -mm-diam Mo disk is buried  $40$   $\mu\text{m}$  behind the target's front surface. The target is oriented in the equatorial plane of the NIF chamber and irradiated by a subset of NIF beams from the south pole. Hot electrons generated by the LPI instability in the coronal plasma flow into the target. Time-resolved  $K_\alpha$  line emission and the hard x-ray bremsstrahlung from Mo are used as the main hot-electron diagnostics. The Mo thickness is equal to the range of electrons of a typical energy of  $\sim 120$  keV. Hot electrons that are not stopped in Mo are slowed down in the back CH, so that electron recirculation is minimal in this experiment. The front CH layer is chosen to be thick enough to avoid a burnthrough to the Mo layer, while sufficiently thin to reduce collisional energy losses of hot electrons on the way toward the Mo. For the proposed target thickness, the laser-induced shock does not reach the back of the target, and the target is not accelerated when the laser pulse is on. The simulations use laser pulses with a 2-ns linear power rise from zero to the maximum value and flattop after that, with a total duration of 5.5 to 7.5 ns.



E24123JR

Figure 145.17  
The proposed target design.

The measurements can be performed using the NIF x-ray spectrometer<sup>11</sup> to measure the time-resolved Mo  $K_\alpha$  emission and the filter-fluorescer x-ray diagnostic<sup>12</sup> to measure the time-resolved hard x-ray emission. NIF optical spectrometers can measure the half-frequency ( $\omega_L/2$ ) harmonic of the incident light, which is a characteristic signature of TPD, and SRS spectra.

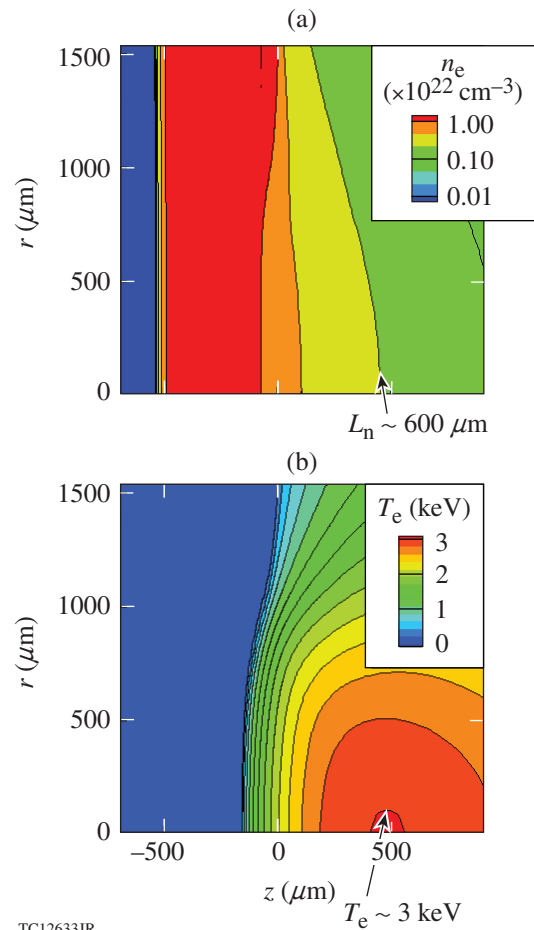
### DRACO Simulations

The simulations were performed using the Eulerian version of *DRACO*<sup>8</sup> in cylindrically symmetric geometry. *DRACO* includes a full three-dimensional (3-D) laser ray trace, a flux-limited heat-conduction model (with a flux limiter  $f = 0.1$ ), multigroup diffusive radiation transport, and *SESAME* equation of state. For the low-Z plastic CH ablator, the Astrophysics

Opacity Table was applied; the average-ion model, which is a collisional-radiative-equilibrium model, was used for the high-Z Mo.

The simulations used the actual measured focal-spot shapes of the indirect-drive NIF beams. The beams are used at best focus and pointed at the averaged-over-time longitudinal position of the  $n_{qc}$  surface— $320$   $\mu\text{m}$  in front of the target surface. The simulations are designed to have similar plasma parameters at the  $n_{qc}$  surface, with flattop total powers of 17 TW and 15 TW, durations of 5.5 ns and 7.5 ns in the inner- (32 beams at  $23.5^\circ$  and  $30^\circ$ ) and outer-cone beam (64 beams at  $44.5^\circ$  and  $50^\circ$ ) simulations, respectively. The duration of the flattop used in the inner-cone beam simulation is chosen to be the longest allowable while still avoiding laser damage on the NIF.

Figure 145.18 presents the electron density and electron temperature in the coronal plasma at  $t = 4.5$  ns in the inner-cone



TC12633JR

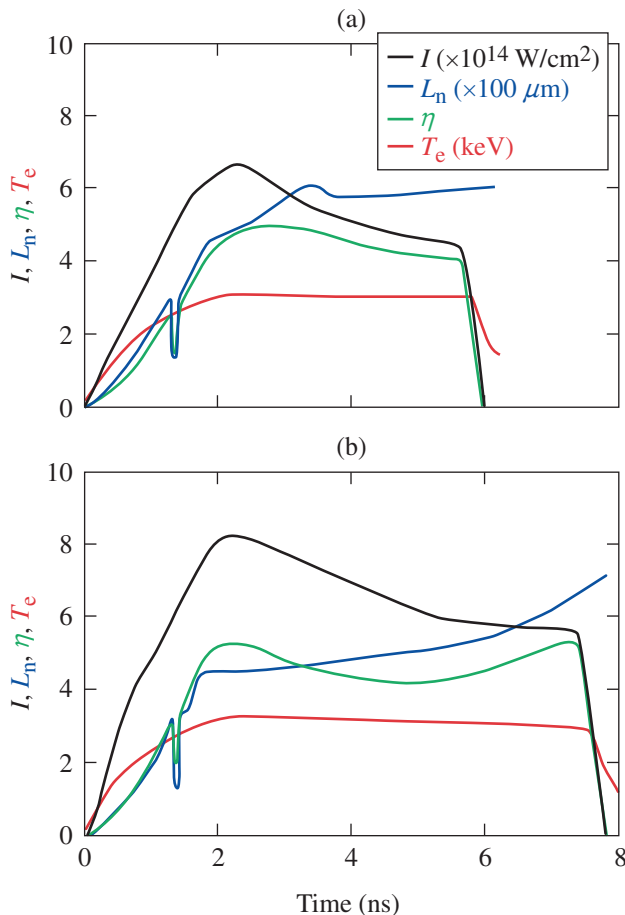
Figure 145.18  
The (a) electron density and (b) electron temperature in the coronal plasma at  $t = 4.5$  ns in the inner-cone beam simulation.

beam simulation. The outer-cone beam simulation predicts similar results (with a slightly higher peak temperature of 3.15 keV) and is not shown.

Figure 145.19 shows the time evolution of the plasma parameters at the  $n_{qc}$  surface and TPD threshold parameter at  $r = 0$  in both simulations. The density scale length and electron temperature are almost stationary at  $t > 2.5$  ns with  $L_n = 500$  to  $600 \mu\text{m}$  and  $T_e \sim 3$  to  $3.3$  keV. Laser intensity slowly decreases with time, with  $I = 5$  to  $6.5 \times 10^{14} \text{ W/cm}^2$  in the inner-cone beam and  $I = 6$  to  $8 \times 10^{14} \text{ W/cm}^2$  in the outer-cone beam simulation. Notably, the empirical TPD threshold is greatly exceeded in these simulations— $\eta \sim 4$  to  $5$ .

### Discussion and Conclusions

Overall, a similar evolution of the plasma parameters at the  $n_{qc}$  surface is predicted by *DRACO* simulations for the inner-



E24123JR2

Figure 145.19 Time evolution of the plasma parameters at the  $n_{qc}$  surface and TPD threshold parameter at  $r = 0$  in the (a) inner- and (b) outer-cone beam simulations.

and outer-cone beams. Planar-target experiments on the NIF, therefore, can study the effect of a beam's incidence angle on TPD instability and hot-electron generation. Simulations of TPD using the 3-D laser-plasma interaction code *LPSE*<sup>13</sup> have been performed using the NIF irradiation geometry and plasma parameters at the  $n_{qc}$  surface predicted by *DRACO*. *LPSE* models the TPD instability in a small volume of plasma ( $200 \mu\text{m} \times 30 \mu\text{m} \times 30 \mu\text{m}$ ) close to the  $n_{qc}$  surface. *LPSE* simulations confirm the onset of TPD instability when the TPD threshold ( $\eta$ ) exceeds unity in *DRACO* simulations for both irradiation geometries. The mechanisms of saturation of the TPD instability (such as pump depletion) are currently under implementation in *LPSE*. *LPSE* will be used to study hot-electron production and laser absorption at the nonlinear stage of TPD.

Table 145.II shows that the plasma parameters at the  $n_{qc}$  surface in the present simulations are closer to the PDD-ignition design than in the OMEGA and current NIF PDD implosion experiments, with the exception of the electron temperature. In particular, the plasma density scale length is as long as that in the ignition design. A relatively low temperature is explained by higher transversal thermoconduction losses in planar experiments compared to those in spherical implosions. The laser power can be further increased, provided the optics' damage threshold is not exceeded. This can allow one to study TPD at higher overlapped laser intensity (equal or exceeding that in the ignition design) and electron temperature at the  $n_{qc}$  surface. The power can be increased by up to a factor of 2 in the outer-beam configuration. The power can also be increased at the expense of decreased pulse duration in the inner-beam configuration.

In conclusion, hydrodynamic simulations suggest that planar-target experiments on the NIF can be a powerful tool in the study of TPD and other LPI processes in the plasma conditions relevant to the ignition direct-drive designs. While current NIF PDD experiments suffer from CBET, which reduces the laser absorption, planar NIF experiments can provide a first look at the effect of TPD in NIF PDD implosions when CBET has been mitigated. Subsequently, the NIF planar platform can be used to study TPD mitigation strategies by using different ablator materials.

### ACKNOWLEDGMENT

This material is based upon work supported by the Department of Energy National Nuclear Security Administration under Award Number DE-NA0001944, the University of Rochester, and the New York State Energy Research and Development Authority. The support of DOE does not constitute an endorsement by DOE of the views expressed in this article.

REFERENCES

1. M. N. Rosenbluth, *Phys. Rev. Lett.* **29**, 565 (1972).
2. A. Simon, R. W. Short, E. A. Williams, and T. Dewandre, *Phys. Fluids* **26**, 3107 (1983).
3. D. T. Michel, A. V. Maximov, R. W. Short, S. X. Hu, J. F. Myatt, W. Seka, A. A. Solodov, B. Yaakobi, and D. H. Froula, *Phys. Rev. Lett.* **109**, 155007 (2012).
4. J. Zhang, J. F. Myatt, R. W. Short, A. V. Maximov, H. X. Vu, D. F. DuBois, and D. A. Russell, *Phys. Rev. Lett.* **113**, 105001 (2014).
5. S. Skupsky, J. A. Marozas, R. S. Craxton, R. Betti, T. J. B. Collins, J. A. Delettrez, V. N. Goncharov, P. W. McKenty, P. B. Radha, T. R. Boehly, J. P. Knauer, F. J. Marshall, D. R. Harding, J. D. Kilkenny, D. D. Meyerhofer, T. C. Sangster, and R. L. McCrory, *Phys. Plasmas* **11**, 2763 (2004).
6. M. Hohenberger, P. B. Radha, J. F. Myatt, S. LePape, J. A. Marozas, F. J. Marshall, D. T. Michel, S. P. Regan, W. Seka, A. Shvydky, T. C. Sangster, J. W. Bates, R. Betti, T. R. Boehly, M. J. Bonino, D. T. Casey, T. J. B. Collins, R. S. Craxton, J. A. Delettrez, D. H. Edgell, R. Epstein, G. Fiksel, P. Fitzsimmons, J. A. Frenje, D. H. Froula, V. N. Goncharov, D. R. Harding, D. H. Kalantar, M. Karasik, T. J. Kessler, J. D. Kilkenny, J. P. Knauer, C. Kurz, M. Lafon, K. N. LaFortune, B. J. MacGowan, A. J. Mackinnon, A. G. MacPhee, R. L. McCrory, P. W. McKenty, J. F. Meeker, D. D. Meyerhofer, S. R. Nagel, A. Nikroo, S. Obenschain, R. D. Petrasso, J. E. Ralph, H. G. Rinderknecht, M. J. Rosenberg, A. J. Schmitt, R. J. Wallace, J. Weaver, C. Widmayer, S. Skupsky, A. A. Solodov, C. Stoeckl, B. Yaakobi, and J. D. Zuegel, *Phys. Plasmas* **22**, 056308 (2015).
7. B. Yaakobi, P.-Y. Chang, A. A. Solodov, C. Stoeckl, D. H. Edgell, R. S. Craxton, S. X. Hu, J. F. Myatt, F. J. Marshall, W. Seka, and D. H. Froula, *Phys. Plasmas* **19**, 012704 (2012).
8. P. B. Radha, T. J. B. Collins, J. A. Delettrez, Y. Elbaz, R. Epstein, V. Yu. Glebov, V. N. Goncharov, R. L. Keck, J. P. Knauer, J. A. Marozas, F. J. Marshall, R. L. McCrory, P. W. McKenty, D. D. Meyerhofer, S. P. Regan, T. C. Sangster, W. Seka, D. Shvarts, S. Skupsky, Y. Srebro, and C. Stoeckl, *Phys. Plasmas* **12**, 056307 (2005).
9. T. J. B. Collins, J. A. Marozas, K. S. Anderson, R. Betti, R. S. Craxton, J. A. Delettrez, V. N. Goncharov, D. R. Harding, F. J. Marshall, R. L. McCrory, D. D. Meyerhofer, P. W. McKenty, P. B. Radha, A. Shvydky, S. Skupsky, and J. D. Zuegel, *Phys. Plasmas* **19**, 056308 (2012).
10. W. Seka, D. H. Edgell, J. F. Myatt, A. V. Maximov, R. W. Short, V. N. Goncharov, and H. A. Baldis, *Phys. Plasmas* **16**, 052701 (2009).
11. S. P. Regan, K. B. Fournier, M. J. Bedzyk, A. Agliata, S. L. Ayers, M. A. Barrios, P. M. Bell, D. K. Bradley, H. Chen, J. A. Emig, R. K. Jungquist, G. E. Kemp, J. D. Kilkenny, D. D. Meyerhofer, F. Perez, J. Pino, T. C. Sangster, and M. J. Shoup III, *SPIE Optics and Photonics 2014*, San Diego, CA, 17–21 August 2014 (Paper 9211-15).
12. M. Hohenberger, F. Albert, N. E. Palmer, J. J. Lee, T. Döppner, L. Divol, E. L. Dewald, B. Bachmann, A. G. MacPhee, G. LaCaille, D. K. Bradley, and C. Stoeckl, *Rev. Sci. Instrum.* **85**, 11D501 (2014).
13. J. F. Myatt, J. G. Shaw, V. N. Goncharov, J. Zhang, A. V. Maximov, R. W. Short, R. K. Follett, W. Seka, D. H. Edgell, and D. H. Froula, “Laser-Plasma Interaction in Direct-Drive Inertial Confinement Fusion,” submitted to the *Journal of Physics: Conference Series*.